Forest structural variables retrieval using EO-1 hyperion data in combination with linear spectral unmixing and an inverted geometric-optical model

Zeng, Yuan ; Schaepman, Michael E ; Wu, Bing-fang ; Clevers, Jan G P W ; Bregt, Arnold K

Article ID: 1007-4619(2007)05-0648-11

Forest Structural Variables Retrieval Using EO-1 Hyperion Data in Combination with Linear Spectral Unmixing and an Inverted Geometric-Optical Model

ZENG Yuan[1,2], Michael E. Schaepman[2], WU Bing-fang[1],
Jan G. P. W. Clevers[2], Arnold K. Bregt[2]
(1. *Institute of Remote Sensing Applications, Chinese Academy of Sciences, Beijing* 100101, *China*;
2. *Centre for Geo-Information, Wageningen University, Wageningen, the Netherlands*)

Abstract: The potential of EO-1 Hyperion data combined with linear spectral unmixing and an inverted geometric-optical model for the retrieval of forest structural variables in the Longmenhe broadleaved forest natural reserve, located in the Three Gorges region(China), is studied in this paper. Based on the principle of Li-Strahler geometric-optical model, we derive the per-pixel reflectance as being a linear combination of four scene components(sunlit canopy/sunlit background and shaded canopy/shaded background). The fraction of each component is subsequently related to several forest structural attributes. With the advantage of having hyperspectral data, we use linear spectral unmixing to separate the above classes present in an atmospherically corrected Hyperion image with support of extensive in situ measurements. In addition, we include DEM derived parameters(slope and aspect) and measured canopy structural parameters for different forest communities to invert the geometric-optical model and retrieve the pixel-based variables forest crown closure(*CC*) and crown diameter(*CD*). In total 37 sample plots collected in the Longmenhe study region are used for validation, and the results of the above parameters show a good agreement(e. g., $R^2_{CC}=0.61/RMSE=0.046$; $R^2_{CD}=0.39/RMSE=0.984$).

Key words: EO-1 hyperion; forest structural variable; crown closure; crown diameter; geometric-optical model; linear spectral unmixing; Three Gorges region
CLC number: TP701 **Document code**: A

1 INTRODUCTION

Human transformations of ecosystems and landscapes are currently one of the largest sources of change on Earth. In particular the provision of ecosystem services, directly affecting human well-being, demand sustainable development and optimal management of natural resources in the coupled human-environment system[1]. Population change, land management decisions and practices-amongst others-affect ecosystem properties and therefore require a sustainable socio-economic development in any region on Earth[2]. Among the various natural resources that are present on the terrestrial Earth surface, forests are one of the most important contributors that influence ecosystems with respect to carbon storage and release[3]. Accurate and up-to-date information on forest structure is essential for many aspects of forest management and changes in forest structure also provide insights related to forest vigor, harvesting, burning, stocking levels, disease, and insect infestations[4]. Thus, quantitatively monitoring forest structure using remote sensing methods strongly supports the conservation and man-

Received date: 2006-08-10; **Accepted date**: 2007-03-15
Foundation item: 'Knowledge Innovation Project' of the Chinese Academy of Sciences(No. KZCX3-SW-334).
Biography: ZENG Yuan, currently a Ph. D. student of the Wageningen University. She has been a staff of the Institute of Remote Sensing Applications since 2003. Her research interests include hyperspectral remote sensing, forest biophysical parameters retrieval and remote sensing applications in forest and crop monitoring. E-mail: yuanz@irsa.ac.cn

agement strategies that take into account biodiversity and the impact of the global carbon cycle.

Main forest structural variables include crown cover, crown size, stem density, tree height, diameter at breast height (DBH), age, spatial distribution, and gap presence etc. Traditionally, quantitative retrieval methods for estimating these variables are grouped into two major categories: statistical and physical approaches. Statistical methods are based mainly on a wide variety of vegetation indices or correlating features and use regression models to infer structural variables directly. Physical methods usually rely on inverting or assimilating canopy reflectance models[5]. An observed trend is that more and more empirical, statistical models are being gradually replaced by physically based models.

Canopy reflectance models have been used to improve mapping of many forest structural variables, particularly geometric-optical models, which regard canopy reflectance as a mixture of discrete canopy components[6]. For example, Hall *et al.* [7] used geometric shadow and linear mixture models to infer several important structural parameters of a boreal forest. Woodcock *et al.* [8,9] estimated the mean tree size and cover for each forest stand through inversion of the Li-Strahler canopy reflectance model in Stanislaus National Forest and found the forest cover estimates more reliable. Gemmell[10] tested the inversion of a geometric-optical forest reflectance model and the utility of two spectral indices (NDVI and SAVI) for estimating crown cover in a conifer forest site. Scarth and Phinn[11] determined the forest crown cover projection, canopy size, tree densities and successional stage using an inverted geometric-optical model in mixed eucalypt forests in Australia. These studies used inversion of the geometric-optical model to monitor forest structural variables are all based on Landsat Thematic Mapper (TM) data. In addition, the authors also suggested that the development of new-generation imaging platforms would provide an opportunity to use multi-angular or hyperspectral remote sensing data for improving and calibrating the inversion of geometric-optical models. Therefore, the objective of this study is to evaluate the benefits of using EO-1 Hyperion hyperspectral data in combination with an inverted geometric-optical model for deriving and mapping two forest structural variables, crown closure (*CC*) and crown diameter (*CD*), in a broadleaved forest.

2 STUDY AREA AND DATA COLLECTION

The study area, namely the Longmenhe forest nature reserve, lies in the Xingshan county of Hubei province, towards the north-east of Three Gorges region in China (centered at 31°20′N, 110°29′E, see Fig. 1). The total reserve size is about 4644 ha and the altitude varies around 1300m above sea level. This study site belongs to the temperate climate zone (Cwa-Subtropical monsoon, Koeppen[12]), average precipitation is about 100—150mm per month and in spring-summer (April-September) season it can be as high as 200—300mm per month. The Longmenhe forest reserve is mainly dominated by about 650 ha natural evergreen broadleaved forest and mixed deciduous broadleaved forest; 223 ha rare plant communities and 121 ha planted subtropical evergreen broadleaved forest.

Field data were collected in April to June of 2003. With support of 1:50000 topographic maps, a total of 40 sample sites (100m × 100m) located in the study area were measured based on different plant strata and topographic distribution, and each of them randomly included 5 sample plots (20m × 20m), which provided relevant photos, plant profile and crown cover maps. Other measurements in each sample plot include the GPS locations and several important forest structural attributes, such as crown diameter and DBH from measuring tape; tree height and trunk height by altimeter; tree age using increment borer; and visual estimations by forest experts for forest type, plant species, crown closure and distribution.

For the study area, a Hyperion image was acquired on June 10, 2004, around 11:00 a. m. local time. Hyperion, one of the three sensors on the NASA EO-1 platform, was launched on November, 2000 and orbited 1min behind Landsat. As a pushbroom imaging instrument, Hyperion provides high resolution hyperspectral images capable of resolving 242 spectral

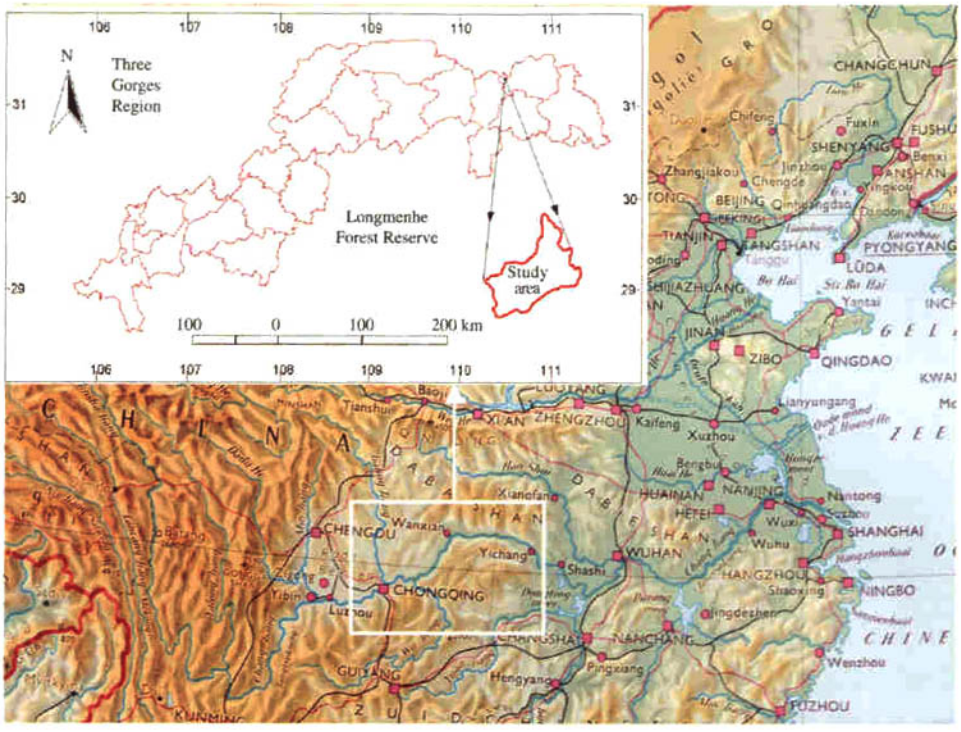

Fig. 1 Location of the Three Gorges region and the study area of Longmenhe forest nature reserve

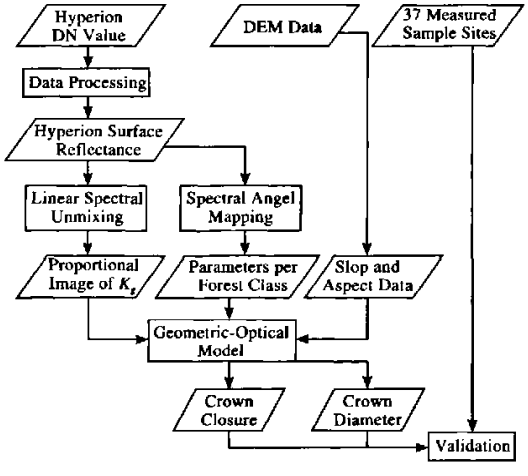

Fig. 2 Flowchart of general methods

bands(from 0.4—2.5μm) with a 10nm spectral resolution and a 30m spatial resolution. Ancillary data also consisted of a digital elevation model(DEM) with 30m spatial resolution, which is required for deriving the model inputs.

3 METHODS

The overall methods used in this study are shown as flowchart in Fig. 2. The sequence involves:

(1) Hyperion data processing, which includes effective band selection, de-striping, radiometric, atmospheric and geometric corrections;

(2) Based on the at-surface reflectance data, deriving the per-pixel proportions of four scene components (sunlit canopy, sunlit background, shaded canopy and shaded background) by linear spectral unmixing analysis;

(3) Using spectral angel mapping to classify the forest with support of field measurements and determine the relevant input parameters;

(4) Inverting the Li-Strahler geometric-optical model integrated with pixel-based sunlit background fraction, canopy structural parameters, slope and aspect data to estimate crown closure and crown diameter;

(5) Quantitatively assessing the accuracy of model retrievals through field data collected for 37 sample sites.

Therefore, the key of this study is the theory of the geometric-optical model.

3.1 Geometric-optical model

The Li-Strahler geometric-optical model[13,14] was derived from the assumption that the Bidirectional Reflectance Distribution Function (BRDF) is a purely geometric phenomenon resulting from a scene of discrete three-dimensional objects being illuminated and viewed from different positions in the hemisphere. The reflectance associated with a given viewpoint is treated as an area-weighted sum of four fixed reflectance components: sunlit canopy (C), shaded canopy (T), sunlit background (G), and shaded background (Z). Therefore, as shown in Fig. 3, for each pixel of a remote sensing image the reflectance (S) can be modeled as a linear combination of four components and their areal proportions (K_g, K_c, K_t and K_z):

$$S = K_g G + K_c C + K_t T + K_z Z \quad (1)$$

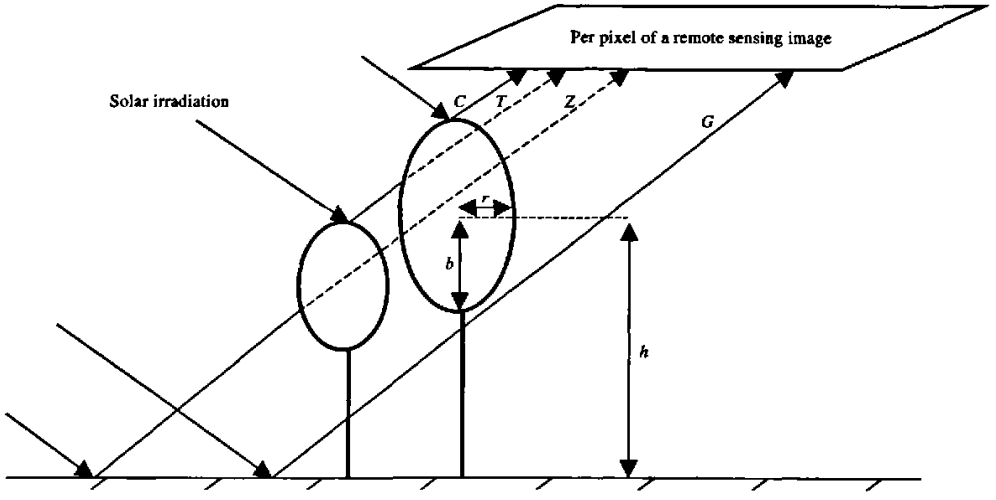

Fig. 3 Per pixel reflectance is modeled as a linear combination of four components (G-sunlit background; C-sunlit canopy; T-shaded canopy and Z-shaded background)

The Li-Strahler model assumes that the resolution of the remote sensing image is much larger than the size of individual crowns but smaller than the size of forest stands, and that the individual trees are randomly (Poisson) distributed within the pixel[15]. Based on the principle of three-dimensional geometry of a spherical crown on a flat background, each proportion of four components can be expressed by a combination of the forest crown structural parameters. For inverting the model, one component (sunlit background) can be used for deriving the expected forest crown closure and crown diameter.

The proportion of sunlit background (K_g) can be formulated using the Boolean model[16]:

$$K_g = e^{-\pi \cdot M \cdot [\sec(\theta_i) + \sec(\theta_v) - O(\theta_i, \theta_v, \varphi)]} \quad (2)$$

Here, $O(\theta_i, \theta_v, \varphi)$ is the average of the overlap function between illumination and viewing shadows of individual crowns as projected onto the background. φ is the difference in azimuth angle between illumination (φ_i) and viewing (φ_v). θ_i, θ_v are the zenith angles of illumination and viewing. M, called the mean of "treeness" parameter m, is defined as $M = \Lambda R^2$, where Λ is the number of trees per unit area.

The exact solution for the overlap function on the principal plane can be determined as[13]:

$$O(\theta_i, \theta_v, \varphi) = 1/\pi(\sec\theta_i + \sec\theta_v)(t - \sin t \cos t) \quad (3)$$

Where t is given by:

$$\cos t = \frac{h|\tan\theta_i - \tan\theta_v \cos\varphi|}{r(\sec\theta_i + \sec\theta_v)} \quad (4)$$

Where t is valued in $[0, \pi/2]$. Therefore, in terms

of equations (2) and (3), M can be inferred as:

$$M = \frac{-\ln(K_g)}{(\sec\theta_i + \sec\theta_v)(\pi - t + \cos t \sin t)} \quad (5)$$

Since M is an important parameter in the relationship between image variables and forest structure, in the case of Poisson distributed trees, the mean crown closure (CC) and crown diameter ($CD = 2 \times R$) can be calculated as follows[9,14]:

$$CC = 1 - e^{-\pi \cdot M} \quad (6)$$

$$R^2 = \frac{\sqrt{(1+\omega)^2 \cdot M^2 + 4 \cdot V(m) \cdot \omega} - (1+\omega) \cdot M}{2\omega} \quad (7)$$

Where, $V(m)$ is the variance of m, and ω is the coefficient of variation of the crown size, which is calculated as the ratio of the mean to the variance of the squared crown radius.

Due to the study area is in the mountain region and actually the crown shape of the broadleaved forest need to be modeled as an ellipsoid, with crown radius (b) in vertical direction, crown radius (r) in horizontal direction and tree height (h) from ground to mid-crown, double transformations are required to allow crowns to be treated as spheres and accommodate the slopping surface. In this study, for nadir viewed status, the illumination, viewing and slope angles are corrected in equations (8) to (16)[17,18].

Transformation from ellipsoid to sphere:

$$\theta_i' = \arctan\left(\frac{\tan\theta_i}{r/b}\right) \quad (8)$$

$$\theta_v' = \arctan\left(\frac{\tan\theta_v}{r/b}\right) \quad (9)$$

$$\theta_s' = \arctan\left(\frac{\tan\theta_s}{b/r}\right) \quad (10)$$

$$h' = (r/b)\, h \quad (11)$$

Slope coordinate system transformation:

$$\theta_i'' = \arccos(\cos(\theta_i')\cos(\theta_s') + \sin(\theta_i')\sin(\theta_s')\cos(\varphi_i - \varphi_s)) \quad (12)$$

$$\theta_v'' = \arccos(\cos(\theta_v')\cos(\theta_s') + \sin(\theta_v')\sin(\theta_s')\cos(\varphi_v - \varphi_s)) \quad (13)$$

$$\varphi_i'' = \arctan(\sin(\theta_i')\sin(\varphi_i - \varphi_s))/(\cos(\theta_i')\cos(\theta_s') + \sin(\theta_i')\sin(\theta_s')\cos(\varphi_i - \varphi_s)) \quad (14)$$

$$\varphi_v'' = \arctan(\sin(\theta_v')\sin(\varphi_v - \varphi_s))/(\cos(\theta_v')\cos(\theta_s') + \sin(\theta_v')\sin(\theta_s')\cos(\varphi_v - \varphi_s)) \quad (15)$$

$$h'' = h'\cos(\theta_s') \quad (16)$$

Finally, the transformed θ_i'', φ_i'', θ_v'', φ''_v, h'' are replaced $\theta_i, \varphi_i, \theta_v, \varphi_v, h$ in equations (4) and (5). Based on equations (6) and (7), the necessary inverted model inputs for determining CC and CD are the proportional image of K_g; the solar zenith and azimuth angles (θ_i, φ_i); the view zenith and azimuth angles (θ_v, φ_v); the local slope and aspect (θ_s, φ_s) and the mean measured parameters for different kinds of forest crown shapes: h, b, r and ω.

3.2 Hyperion data processing

The currently used Hyperion Level 1B1 data have 242 bands of which 196 are nonzero and not overlapping. For converting DNs to radiances ($W/m^2 \cdot sr \cdot \mu m$), the data were scaled by 40 for VNIR and 80 for SWIR (Radiance for VNIR = DN/40; Radiance for SWIR = DN/80)[19]. Several stripes (data columns of poor quality) in the Hyperion data contain no information and lower radiance. Those abnormal pixels are detected and replaced by the average radiance value of their immediate left and right neighboring pixels[20]. The steps are comparing each pixel's value with its neighbors horizontally in each band, if the value is smaller than both neighbors this pixel is labeled as abnormal. Then the numbers of consecutive abnormal pixels is counted vertically, if the percentage of abnormal pixels in each column is greater than 55%, it will be treated as striping and be recalculated by the mean of their neighbors. In addition, a Minimum Noise Fraction (MNF) process can reduce the noise of a hyperspectral image[21]. Based on the Eigenvalue profile, the effective bands containing the most information are selected to obtain the final Hyperion data for model inversion.

Remote sensing data with accurate surface reflectance values are essential for a successful inversion of a canopy reflectance model. Thus, an atmospheric correction is required prior to data analysis. In this study, we use ACORN version 4.0, a commercially available atmospheric correction program based on MODTRAN 4 radiative transfer code[22]. ACORN uses two water absorption channels (940 and 1140nm) in Hyperion data to evaluate the amount of water vapor in combination with the visibility at the moment of data

acquisition. Due to the low signal to noise ratio at the beginning and the end of the spectra ($\leqslant$436nm and $\geqslant$2385nm) and the heavy water absorption influences in several bands, a total of 64 bands are dropped from 196 valid bands. Geometric correction is done by 26 GCPs (Ground Control Points) relative to 1:50000 topographic maps and the geometric error is less than one pixel. Finally, the corrected Hyperion data with 132 bands of surface reflectance in a UTM Zone 49 N WGS-84 projection are used in this study.

3.3 Linear spectral unmixing

Linear spectral unmixing has been widely used to calculate the percentages of several individual surface components contained in each pixel of a remote sensing image[23,24]. The method assumes that the reflectance (S) from each pixel is a linear combination of each endmember (E), which is the pure reflectance spectrum of a surface component. The general equations are

$$S_j = \sum_{i=1}^{n} K_i E_{i,j} \tag{17}$$

$$1 = \sum_{i=1}^{n} K_i \tag{18}$$

Where n is the number of components; j is the bands and K is the fractional abundance of an endmember. In this study, on the basis of the Li-Strahler model, there are only four components (equation (1), G, C, T, and Z) contained in one pixel. Hence, the sum of the four proportions is equal to 1:

$$K_g + K_c + K_t + K_z = 1 \tag{19}$$

Since the proportional image of K_g (sunlit background fraction) is required for inverting the model, selection of the suitable endmembers G, C, T, and Z is the most important issue. Usually, the endmembers are obtained from the observation of a field spectrometer, or are taken directly from a remote sensing image with sufficient field data, or from an existing spectral library. In this case, with the support of extensive in situ measurements, we select the four endmembers by trial and error from Hyperion training samples.

3.4 Spectral angel mapping

Spectral angle mapping (SAM) is one kind of algorithms for classifying hyperspectral data. In SAM, classification is carried out through comparing image spectra to individual endmembers. The similarity between an endmember and the per-pixel image spectrum is determined by calculating the "spectral angle", treating them as vectors in a space with a dimensionality equal to the number of bands. If the spectral angle between them is very small, it implies that the pixel is close to this endmember[25].

SAM is used for forest classification in the Longmenhe study area for determining the required model inputs of the pixel-based forest crown shape parameters. Thanks to every homogeneous forest region is much more than one pixel of 30m, the endmembers representing the different dominant forest communities and species could be detected directly from Hyperion data based on the field measurements. For each pixel of the image, the spectral angles comparing with each endmember are calculated and then the pixel will be assigned to the class of endmember with the smallest angle. We use a standard angle threshold of 0.1 radians to identify unclassified pixels. The accuracy of SAM classification is estimated by a confusion matrix based on 40 independent field sample sites.

4 RESULTS

4.1 Model input data

The processed Hyperion data with surface reflectance is shown in Fig.4(a). Because of the cloud cover affecting the quality of this image, finally we use an image subset of size 208(column) $\times$173(line) $\times$132(band). After comparing the typical spectral library and analyzing the training samples collected from the fieldwork, such as a small playground of a primary school, a bare farming place, closed and open forest regions, etc., the purest pixels representing the endmembers of four components, sunlit background G, sunlit canopy C, shaded canopy T and shaded background Z, are selected from the Hyperion image(Fig.5). Combined with equation (1) and (19), the areal proportions of K_g, K_c, K_t and K_z are calculated for each pixel, and the proportional image of K_g is shown in Fig.4(b). The brighter regions express higher

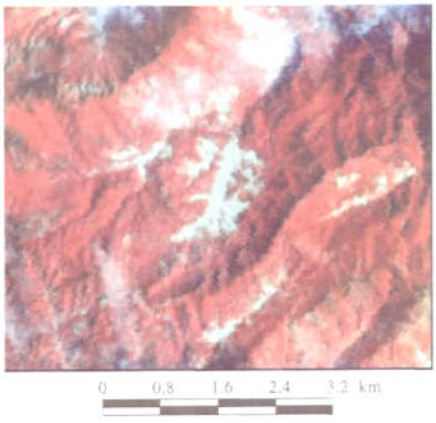

(a) Hyperion image(Bands R:50 G:23 B:16)

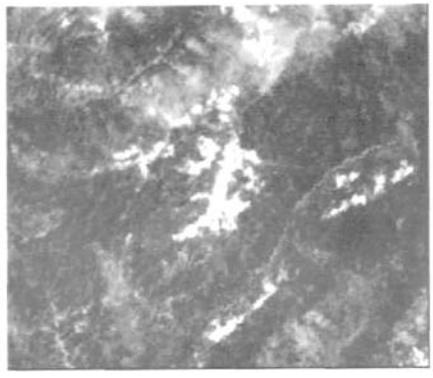

(b) Proportional image of K_g

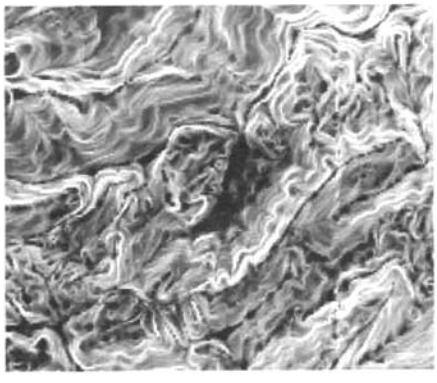

(c) Slope data with 30m resolution

(d) Aspect data with 30m resolution

Fig.4 Processed Hyperion data and necessary inputs for inversion of the Li-Strahler model

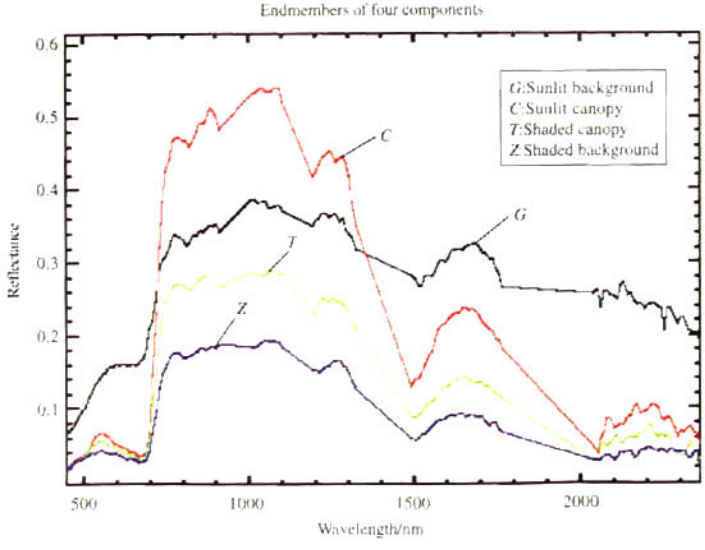

Fig.5 Four Endmembers derived from the Hyperion image

proportions. Here, we assume $0 \leqslant K_g \leqslant 1$, although a few pixels in the linear spectral unmixing approach produced negative fractions, which subsequently are recoded as infeasible areas with no data in the final mapping results.

As mentioned at the end of section 3.1, besides the proportion K_g, the other required inputs for inversion of the Li-Strahler model, slope and aspect images are derived from DEM data using topographic analysis model of ERDAS IMAGINE, see Fig. 4(c)—(d). In addition, this nadir viewed Hyperion image was acquired at a 23.5° solar zenith and 104.5° solar azimuth angle.

4.2 Forest classification

In this study area, the dominant forest communities include deciduous broadleaved forest, evergreen broadleaved forest, and conifer forest. Most of the collected field sample sites(100m × 100m) were chosen in a homogeneous forest with different predominant species. Finally, 7 pixels indicating the typical forest classes' spectra as endmembers are detected from the Hyperion image. Those are DP: Deciduous broadleaved forest-*Platacarya strobilacea*; DQ: Deciduous broadleaved forest-*Quercus glandulifera var. brevipetiolata*; DB: Deciduous broadleaved forest-*Betula luminifera*; CP: Conifer forest-*Pinus tabulaeformis tabulaeformis*; CL: Conifer forest-*Larix keaempferi*; EQ: Evergreen broadleaved forest-*Quercus spinosa* and EC: Evergreen broadleaved forest-*Cyclobalanopsis oxyodon*. The forest classification result by applying the SAM algorithm is shown in Fig. 6.

We separately recode the deciduous broadleaved forest (DBF), evergreen broadleaved forest (EBF), and conifer forest (CF) into class 1, 2 and 3, respectively. We consider class 0 as being unclassified pixels, when a SAM distance of more than 0.1 radians has been calculated comparing to the remaining other 7 endmembers. Class 0 includes both the non-forested regions as well as regions that were affected by clouds or shadows. Using 40 field sample sites to validate the SAM forest classification result, the confusion matrix(Table 1) indicates that the percentage of correct classification reaches 78%. In terms of the field measurements, the corresponding mean value of forest crown parameters, h, b, r and ω for every dominant forest class is shown in Table 2.

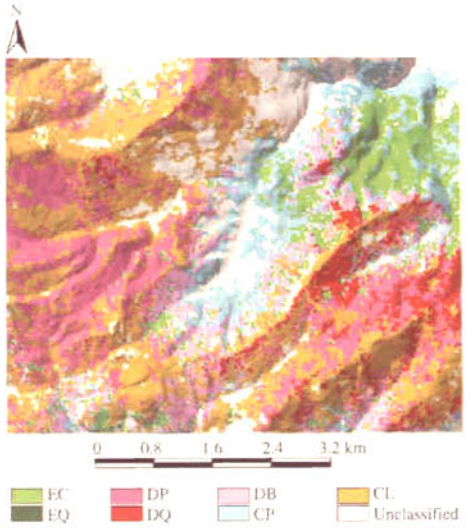

Fig. 6 Forest classification result using the SAM algorithm

Table 1 Confusion matrix of the SAM forest classification result

Field measurements (40 samples)	SAM classes			Total	Accuracy/%
	DBF	EBF	CF		
Deciduous Broadleaved Forest	17	3	1	21	81
Evergreen Broadleaved Forest	2	8	0	10	80
Conifer Forest	2	1	6	9	67
Total	21	12	7	31/40	78

Table 2 Inverted model inputs for each forest class

Dominant Forests	h/m	b/m	r/m	ω
Deciduous Broadleaved Forest	9.79	3.97	1.79	1.25
Evergreen Broadleaved Forest	8.86	3.36	1.61	3.02
Conifer Forest	8.41	4.63	1.51	1.87

4.3 Model output and validation

We design and compile an IDL program to implement the inversion of the Li-Strahler model integrated with the pixel-based input data. Fig. 7 presents the final mapping results of forest structural variables, crown closure(CC) and crown diameter(CD), distributed in the Longmenhe study area.

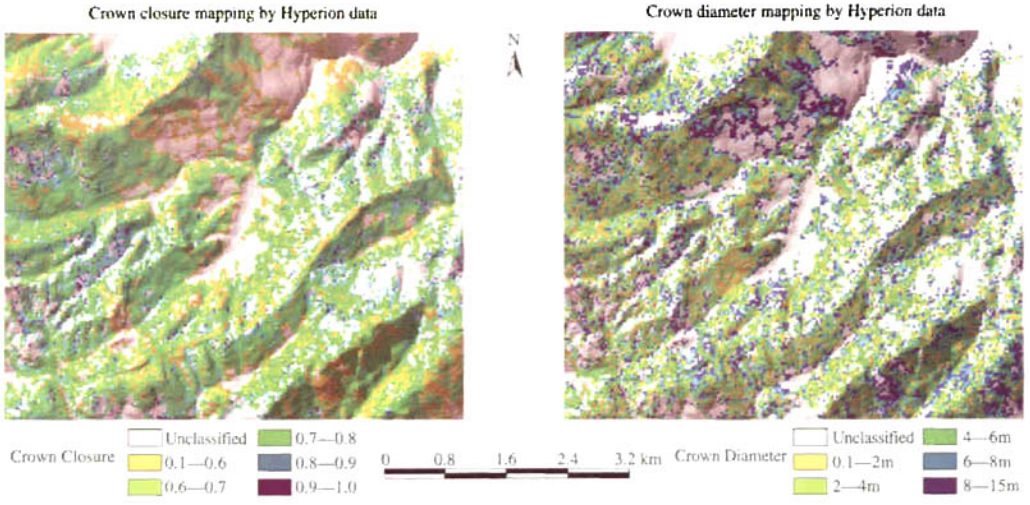

Fig. 7 Mapping results of forest crown closure (*CC*) and crown diameter (*CD*) by the inverted geometric-optical model

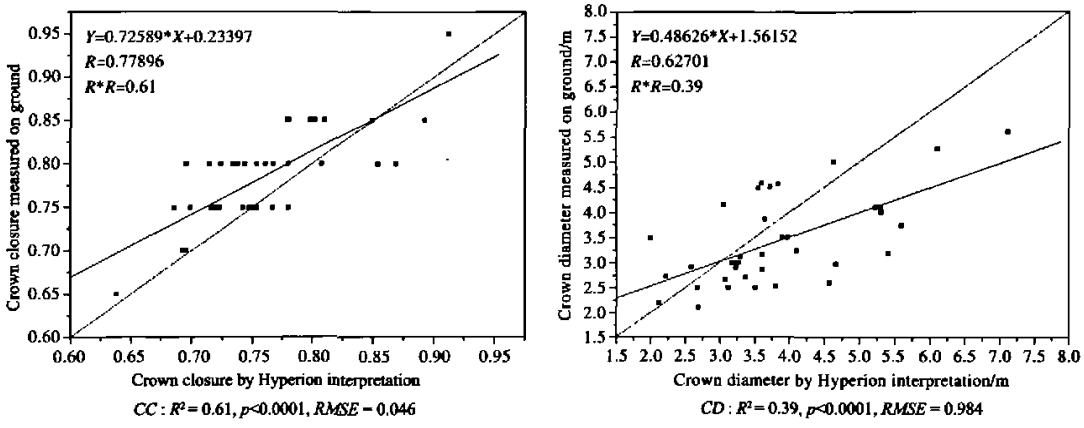

Fig. 8 Linear relationship between ground measured *CC/CD* and model derived *CC/CD*

For validating the model outputs, we use the mean value of a 3 × 3 window for comparison to one field sample site. Fig. 8 illustrates the agreement between model-interpreted *CC/CD* and ground-measured values. In total 37 valid independent samples are included. The closer the points to the 1∶1 line, the better the predicted results are. The coefficient of determination R^2 is equal to 0. 61 for *CC* and 0. 39 for *CD*, $p < 0.0001$. The calculated root mean squared error is $RMSE_{CC} = 0.046$ and $RMSE_{CD} = 0.984$. Although most of the interpreted results of *CC* seem to be less than the field measured values as well as the values of *CD* partly do not match the ground data very well, the reliability of model output is considered to be acceptable.

5 CONCLUSION AND OUTLOOK

The inverted geometric-optical model combined with the spectral unmixing analysis used in this study proved to be useful to derive forest canopy structural variables from Hyperion data in the Longmenhe broadleaved forest. The accuracy of the inverted model results mainly depends on the detectability of M('treeness'). Thus, as shown in equation (5), for a better calibration of the model, a sensitivity analysis may be performed, estimating the sensitivity of M to the sunlit background fraction (K_s), the crown shape parameters

r/b, *h/b* and the calculated slope/aspect angles.

The accuracy of both, the forest classification and the field measurements are substantially influencing the model input parameters. Several methods using hyperspectral data based classification approaches have been documented in literature, and this contribution positions itself well in the generally achieved classification accuracies. However, choosing 37 sample sites for validating the model results has been found to be at the lower limit to achieve successful model accuracies. We will in the future investigate, if high spatial resolution data can increase the model accuracy by combining these two approaches.

We evaluated the use of spaceborne imaging spectrometer data in combination with a physical-based canopy reflectance model to determine forest structural variables at regional scale to be efficient and useful. Even though selected procedures will need more careful analysis in the future, the presented results show confidence in the approach selected. Besides the crown closure and crown diameter variables, other forest structural and biophysical attributes, like stem density, tree height, DBH, age and LAI, can also possibly be estimated more exactly by the inversion of canopy reflectance models with support of high spatial and hyperspectral remote sensing data. Consequently, quantitative monitoring the forest ecosystem and its changes over time using effective and coherent models will be a major future goal.

ACKNOWLEDGMENT

We appreciate support from Xu Wenting, Huang Jianxi and Tian Yichen for participation in the field campaign. We thank the anonymous reviewers for helpful suggestions and comments.

REFERENCES

[1] GLP. Science Plan and Implenetation Strategy[R]. IGBP Report No. 53/IHDP Report No. 19., I. Secretariat, Editor. Stockholm, 2005.

[2] Murai S. Applications of Remote Sensing in Asia and Oceania-Environmental Change Monitoring[A]. Asian Association on Remote Sensing, Tokyo, 1991.

[3] Schimel D S, House J I, Hibbard K A, *et al*. Recent Patterns and Mechanisms of Carbon Exchange by Terrestrial Ecosystems [J]. *Nature*, 2001, **414**(6860): 169—172.

[4] Wulder M. Optical Remote-Sensing Techniques for the Assessment of Forest Inventory and Biophysical Parameters[J]. *Progress in Physical Geography*, 1998, **22**(4): 449—476.

[5] Liang S. Quantitative Remote Sensing of Land Surfaces[A]. Wiley Series in Remote Sensing[C]. Hoboken, NJ: Wiley-Interscience 2004, XXVI, 534.

[6] Ustin S L. Remote Sensing for Natural Resource Management and Environmental Monitoring[A]. Hoboken, NJ: Wiley, 2004, XXXII, 736.

[7] Hall F G, Shimabukuro Y E, Huemmrich K F. Remote-Sensing of Forest Biophysical Structure Using Mixture Decomposition and Geometric Reflectance Models[J]. *Ecological Applications*, 1995, **5**(4): 993—1013.

[8] Woodcock C E. Estimation of Forest Stand Structure from Landsat TM Through Inversion of the Li-Strahler Model[A]. International Geoscience and Remote Sensing Symposium (IGARSS)[C]. 1994.

[9] Woodcock C E, Collins J B, Jakabhazy VD, *et al*. Inversion of the Li-Strahler Canopy Reflectance Model for Mapping Forest Structure[J]. *IEEE Transactions on Geoscience and Remote Sensing*, 1997, **35**(2): 405—414.

[10] Gemmell F. Estimating Conifer Forest Cover with Thematic Mapper Data Using Reflectance Model Inversions and Two Spectral Indices in a Site with Variable Background Characteristics [J]. *Remote Sensing of Environment*, 1999, **69**(2): 105—121.

[11] Scarth P, Phinn S. Determining Forest Structural Attributes Using an Inverted Geometric-Optical Model in Mixed Eucalypt Forests, Southeast Queensland, Australia[J]. *Remote Sensing of Environment*, 2000, **71**(2): 141—157.

[12] McKnight T L, Hess D. Climate Zones and Types: Dry Humid Subtropical Climate(Cfa, Cwa)[A]. Physical Geography: A Landscape Appreciation. Upper Saddle River, NJ: Prentice Hall, 2000.

[13] Li X W, Strahler A H. Geometric-optical Bidirectional Reflectance Modeling of the Discrete Crown Vegetation Canopy: Effect of Crown Shape and Mutual Shadowing[J]. *IEEE Transactions on Geoscience and Remote Sensing*, 1992, **30**: 276—292.

[14] Li X W, Strahler A H. Geometric-optical Modeling of a Conifer Forest Canopy[J]. *IEEE Transactions on Geoscience and Remote Sensing*, 1985, **23**(5): 705—721.

[15] Woodcock C E, Collins JB, Gopals, *et al*. Mapping Forest Vegetation Using Landsat TM Imagery and a Canopy Reflectance Model[J]. *Remote Sensing of Environment*, 1994, **50**(3): 240—254.

[16] Strahler A H, Jupp D L B. Modeling Bidirectional Reflectance of Forests and Woodlands Using Boolean Models and Geometric Optics[J]. *Remote Sensing of Environment*, 1990, **34**(3): 153—166.

[17] Schaaf C B, Li X W, Strahler A H. Topographic Effects on Bidirectional and Hemispherical Reflectances Calculated with a Geometric-Optical Canopy Model[J]. *IEEE Transactions on Geoscience and Remote Sensing*, 1994, 32(6): 1186—1193.

[18] Li X W, Wang J D. Vegetation Optical Remote Sensing Models and Vegetation Structure Parameterization[M]. Beijing: Science Press, 1995.

[19] Beck R. EO-1 User Guide-Version 2.3. Satellite Systems Branch, USGS Earth Resources Observation Systems Data Center (EDC), 2003.

[20] Han T, Goodenough D G, Dyk A, *et al*. Detection and Correction of Abnormal Pixels in Hyperion Images[A]. International Geoscience and Remote Sensing Symposium (IGARSS)[C]. 2002.

[21] Green A A, Berman M, Switzer P, *et al*. A Transformation for Ordering Multispectral Data in Terms of Image Quality with Implications for Noise Removal[J]. *IEEE Transactions on Geoscience and Remote Sensing*, 1988, 26(1): 65—74.

[22] AIG. ACORN 4.0 User's Guide. Boulder, CO: Analytical Imaging and Geophysics LLC, 2002.

[23] Peddle D R, Hall F G, LeDrew E F. Spectral Mixture Analysis and Geometric-Optical Reflectance Modeling of Boreal Forest Biophysical Structure[J]. *Remote Sensing of Environment*, 1999, 67(3): 288—297.

[24] Goodwin N, Coops N C, Stone C. Assessing Plantation Canopy Condition from Airborne Imagery Using Spectral Mixture Analysis and Fractional Abundances[J]. *International Journal of Applied Earth Observation and Geoinformation*, 2005, 7(1): 11—28.

[25] Zeng Y. Using Hyperspectral Data for Identifying Geological and Soil Units in the Alora Region, Southern Spain[R]. Thesis report, Centre for Geo-information, Wageningen University and Research Centre, GIRS-2003-23, 2003, 57.

基于高光谱遥感数据提取森林结构参数的研究

曾 源[1,2], Michael E. Schaepman[2], 吴炳方[1], Jan G. P. W. Clevers[2], Arnold K. Bregt[2]

(1. 中国科学院 遥感应用研究所 农业与生态遥感研究室, 北京 100101;
2. Centre for Geo-Information, Wageningen University, Wageningen, the Netherlands)

摘 要: 以位于三峡库区的龙门河森林自然保护区为研究区,综合利用线性光谱混合模型和几何光学模型,基于高光谱遥感数据提取森林结构参数是本文研究的重点。在研究区地面调查数据的基础上,通过高光谱数据和混合光谱分解法,获得反演几何光学模型所需的四分量参数,根据背景光照分量与森林植被冠层各参数间的关系,反演得到森林冠层郁闭度及平均冠幅的定量分布图,并利用37个野外实测样本进行结果验证。

关键词: 高光谱; 森林结构参数; 郁闭度; 冠幅; 几何光学模型; 线性光谱混合模型; 三峡库区